NASA TECHNICAL MEMORANDUM

NASA TM X-73675

NASA TM X-73675

ATMOSPHERIC OZONE MEASUREMENTS MADE FROM B-747 AIRLINERS: SPRING 1975

by P. D. Falconer, J. D. Holdeman, and A. D. Taylor
Lewis Research Center
Cleveland, Ohio 44135

TECHNICAL PAPER presented at the
Joint Symposium on Atmospheric Ozone
cosponsored by the International Association of Meteorology and Atmospheric Physics, the World Meteorological Organization, and the International Association of Geomagnetism and Aeronomy
Dresden, German Democratic Republic, August 9-17, 1976

ATMOSPHERIC OZONE MEASUREMENTS MADE FROM B-747 AIRLINERS: SPRING 1975

by P. D. Falconer*, J. D. Holdeman**, and A. D. Taylor*

ABSTRACT

Atmospheric ozone in the upper troposphere and lower stratosphere north of the equator has been registered aboard two commercial B-747 airliners during the Spring of 1975. This monitoring is part of a much broader and continuing project developed by NASA and known as the Global Atmospheric Sampling Program (GASP). Additional flight and meteorological conditions have also been automatically recorded on board concurrent with the ozone measurements. Independently-derived tropopause pressure information was available from NMC data archives and was used to identify stratospheric and tropospheric flight. The composite ozone, flight and meteorological data are reported for selected dates in March, April, and May. Attention is drawn particularly to the vertical profiles of atmospheric ozone mixing ratio as a function of both distance from the tropopause and curvature of the streamlines. The GASP observations suggest that ozone levels typical of the lower stratosphere are often embedded in the upper troposphere, principally during occasions when cyclonic wind curvature was noted.

*NOAA Air Resources Laboratories, Silver Spring, Maryland 20910.
**NASA Lewis Research Center, Cleveland, Ohio 44135

STAR Category 45

ATMOSPHERIC OZONE MEASUREMENTS MADE FROM B-747 AIRLINERS: SPRING 1975

by

P. D. Falconer*, J. D. Holdeman, and A. D. Taylor*

Lewis Research Center

SUMMARY

Atmospheric ozone in the upper troposphere and lower stratosphere north of the equator has been registered aboard two commercial B-747 airliners during the Spring of 1975. This monitoring is part of a much broader and continuing project developed by NASA and known as the Global Atmospheric Sampling Program (GASP). Additional flight and meteorological conditions have also been automatically recorded on board concurrent with the ozone measurements. Independently-derived tropopause pressure information was available from NMC data archives and was used to identify stratospheric and tropospheric flight.

The composite ozone, flight and meteorological data are reported for selected dates in March, April, and May. Attention is drawn particularly to the vertical profiles of atmospheric ozone mixing ratio as a function of both distance from the tropopause and curvature of the streamlines. The GASP observations suggest that ozone levels typical of the lower stratosphere are often embedded in the upper troposphere, principally during occasions when cyclonic wind curvature was noted.

INTRODUCTION

The NASA Global Atmospheric Sampling Program (GASP) has, during the past year and a half, provided a means of retrieving atmospheric ozone and other trace constituent data in the lower stratosphere and

*NOAA Air Resources Laboratories, Silver Spring, MD.

upper troposphere over commercial air routes; the details of the scope of this program may be found elsewhere {1,2,3}. Two of the GASP-equipped, commercial B-747 airliners, one each from the fleet of Pan American World Airways and United Airlines, have provided the data base for this study. The United aircraft collected data over the contiguous United States while the Pan Am 747 provided coverage outside the U.S. on its trans-Atlantic to Europe and trans-Pacific to the Orient routes. The GASP ozone instrument is a U.V. ozone photometer, capable of monitoring ozone amounts from 3 to 20,000 ppbv with a sensitivity of 3 ppbv. A more detailed accounting of the total GASP system design, the measurement instruments, the on-board computer for automatic control and data management, and system maintenance procedures are described in Reference {4}. Finally, the tropopause pressures were obtained from the gridded data archives at the National Meteorological Center (NMC) and were time and space interpolated at each GASP measurement location.

This report presents an exemplary case study for one long-haul flight in March and examines a number of vertical ozone mixing ratio profiles under differing streamline curvatures for selected dates in March, April, and May 1975. All data for these flights were obtained between the altitudes of 8- and 12-km, corresponding to pressure altitudes between 350- and 190-mb. The incremental pressure difference between the NMC-tropopause surface and the aircraft flight level provided the basis for determining vertical ozone profiles. A simple, theoretical treatment of the wind vectors registered on board permitted an ozone profile to be stratified

according to cyclonic or anticyclonic turning of the streamlines. A brief discussion of these observations in light of previous investigations is offered.

THE GASP FLIGHT RECORDS

In order to best portray the interrelationships between the GASP and flight data as a function of aircraft position, longitude-time plots for each flight route were constructed. Figure 1 represents such a display for the Pan Am aircraft, westbound from San Francisco, California to Frankfurt, Federal Republic of Germany via the Far and Middle East. The actual airport destinations enroute are depicted in the uppermost plot box. The ozone mixing ratio (ppbv), the flight pressure-altitudes, and the time-space interpolated tropopause pressures are given in the lower portion of the figure. Finally, the in-flight, ambient temperatures and measured wind vectors are included in the middle plot window. In general, by inspecting (1) rapid step increases and decreases of the ozone mixing ratio, as well as (2) intersection points between the flight altitude and tropopause surface, an estimate of aircraft entrances into the exits from the stratosphere may be made. In many instances, the temperature profile may also be used as a third criterion for identifying stratospheric or tropospheric flight. These features appear in succession in Fig. 1 and are characteristic of each of the springtime flights used in the investigation. The reader may wish to refer to a more complete compilation of GASP records in a report by Holdeman and Falconer {5}. It is worthwhile to mention one important question concerning the high ozone values

found beneath the time-space interpolated tropopause. Occasionally, ozone mixing ratios $\geq$ 150 ppbv, typical of the lower stratosphere during these months, are registered beneath the objectively-derived tropopause. Danielsen {6} and Danielsen and Mohnen {7} discuss the short-comings of conventional tropopause analyses in investigating the exchange of atmospheric tracers between the stratosphere and troposphere. It should be noted that the discrepancies which appeared during the Spring of 1975 were principally associated with trough waves in the upper atmosphere. Particularly intense, three-dimensional deformation fields are often embedded within these large wave disturbances; the organized structure of these motions permit stratospheric tracers to be flushed into the upper troposphere within thin filaments with little loss due to dilution by entrainment.

VERTICAL OZONE PROFILES

During the spring flight series approximately 450 ozone observations were selected for vertical profile analysis. Each datum point was identified as having been obtained within either a cyclonically - or anticyclonically rotating, streamline field by means of the following formulation:

$$K_s = \frac{d\eta}{ds} = \cos(\psi - \nu)\left[\frac{d\nu}{ds_a} - \frac{\sin\psi \tan\phi}{R}\right] + \frac{\sin(\psi - \nu)}{W}\left[\frac{dw}{ds_a}\right]$$

Where $(\psi - \nu)$ = The angle, clockwise, between the aircraft heading and the direction of wind flow,

$\frac{d\nu}{ds_a}$ = Change of wind direction from north along the flight path,

$\frac{\sin\psi\tan\phi}{R}$ = The rate of change of the north vector along the flight path, and

$\frac{I}{w}\frac{dw}{ds_a}$ = rate of change of the wind speed, w, along the flight path.

A complete, mathematical deviation of this equation appears in the Appendix.

This treatment does not explicitly include the effects of wind divergence or shear vorticity across the flight path; that is, the observed wind vectors were treated as non-divergent and irrotational. The sign of the K_S term is defined positive for cyclonic motion, negative for anticyclonic motion. The GASP flight records were scanned, the magnitude and sign of the radii of curvature ($R_S = 1/K_S$, in km) determined, and the corresponding ozone mixing ratios plotted with respect to the tropopause. The results are reproduced in Figs. 2-5.

The one consistent feature in each plot is the differing character of the ozone gradient, $\frac{\Delta O3}{\Delta P}$, above (positive pressure increments) and below the indicated tropopause reference level. The ozone increase within the stratosphere is marked by a large scatter of the data; however, in the upper troposphere, at flight levels at least 40-mb below the tropopause, the observations appear to cluster around mixing ratios between 50-150 ppbv with no marked vertical gradient. In the region immediately below the tropopause surface, the ozone mixing ratios are widely scattered, particularly where streamline curvatures are indicated as cyclonic. As pointed out in the previous section, positive streamline curvature is generally associated with a lower tropopause and the potential for more intense stratospheric-tropospheric exchange. Danielsen has offered one of the few careful analyses of atmospheric structure and aircraft ozone observations for a well-developed cyclone system. It is clear from this one particular case study that ozone mixing ratios can vary by nearly a factor of five just below the *conventionally-analyzed* tropopause. By developing the concept of a *folded tropopause* within which stratospheric

air is embedded, Danielsen showed how and on what scale downward ozone transport can proceed beneath the NMC-coded tropopause. The apparent ambiguity of the GASP ozone records, particularly where cyclonic streamline curvature is indicated, may be best resolved in terms of this exchange mechanism.

Although the data base for this study is too small to quantitatively assess the intermonthly ozone profile variations, it would initially appear that the early spring records (Figs. 2-4) exhibit greater scatter in the upper troposphere than those of April and May (Fig. 5). Whether or not this reflects a greater proportion of cyclone development along the GASP flight routes during March 1975 than in succeeding months has not yet been established. Finally a comment should be made regarding the more well-behaved distribution of ozone about the tropopause for anticyclonic curvature. Negative streamline curvature is generally indicative of a higher tropopause level. The sharp transition from a deep layer of large average stability to a deep layer of small average stability is also characteristic of a high tropopause. The GASP ozone profiles seem to reflect this rapid discontinuity very near to the NMC-derived tropopause surface.

CONCLUDING REMARKS

An evaluation of the vertical distribution of ozone mixing ratios relative to the NMC tropopause surface for a series of Spring flights aboard commercial airliners has been made. The profile data obtained aboard the GASP-equipped aircraft included some 450 observations from a variety of commercial air routes in the Northern Hemisphere. It was found that ozone mixing ratios may be effectively stratified according to the curvature of the wind field, exposing those synoptic conditions

which seem to favor extrusion of ozone-rich air out of the stratosphere into the troposphere. This feature appears in the GASP ozone data for cyclonic streamline rotation where ozone values between 100 and 500 ppbv were registered in the 40-mb layer immediately below the NMC tropopause. No similar ozone variability was recorded for anticyclonic wind rotation.

REFERENCES

{1} Perkins, P.J. and G.M. Reck: Atmospheric Constituent Measurements Using Commercial 747 Airliners. Presented at the ISA Second Joint Conference on the Sensing of Environmental Pollutants. Washington, D.C., December 10-12, 1973. (NASA TM X-71469, 1973).

{2} Reck, G.M., D. Briehl, and P.J. Perkins: Flight Test of a Pressurization System Used to Measure Minor Constituents from an Aircraft. NASA TN D-7576, 1974.

{3} Falconer, P.D. and J.D. Holdeman: Measurements of Atmospheric Ozone Made from a GASP-Equipped 747 Airliner: Mid-March, 1975. Geophys. Res. Lett., Vol. 3, No. 2, 101-104, 1976.

{4} Perkins, P.J. and U.R.C. Gustafsson: An Automated Atmospheric Sampling System Operating on 747 Airliners. Presented at the IEEE International Conference on Environmental Sensing and Assessment. Las Vegas, Nevada, September 14-19, 1975. (NASA TM X-71790).

{5} Holdeman, J.D. and P.D. Falconer: An Analysis of Atmospheric Ozone Measurements Made from a 747 Airliner During March 1976. To be published as a NASA Technical Note.

{6} Danielsen, E.F.: Stratospheric-Tropospheric Exchange Based on Radioactivity, Ozone and Potential Vorticity. J.A.S., Vol. 25, 502-518, 1968.

{7} Danielsen, E.F. and V.A. Mohnen: Project Duststorm Report: Ozone Measurements and Meteorological Analyses of Tropopause Folding. Presented at the IAOC/ICACGP Joint Symposium on Atmospheric Ozone. Dresden, GDR, 9-17 August 1976.

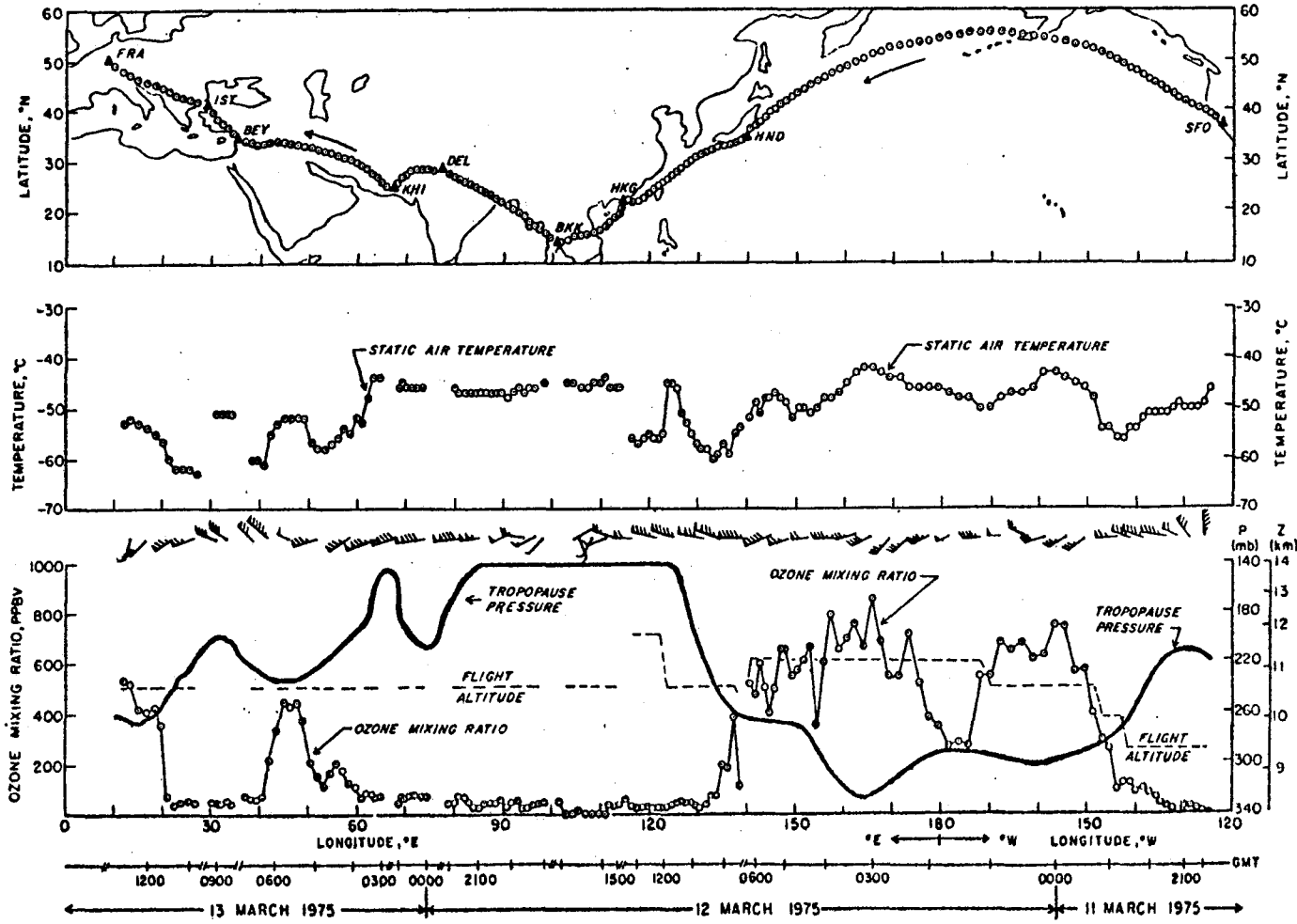

Figure 1. Flight record of 11-13 March 1975 from San Francisco to Frankfurt, F.R.G. Ozone mixing ratios, ambient air temperature, wind data, flight route and altitude are obtained from GASP and aircraft systems. Wind barbs follow standard NWS plotting conventions. Tropopause pressures, obtained from the NMC data archives, have been interpolated in space and time.

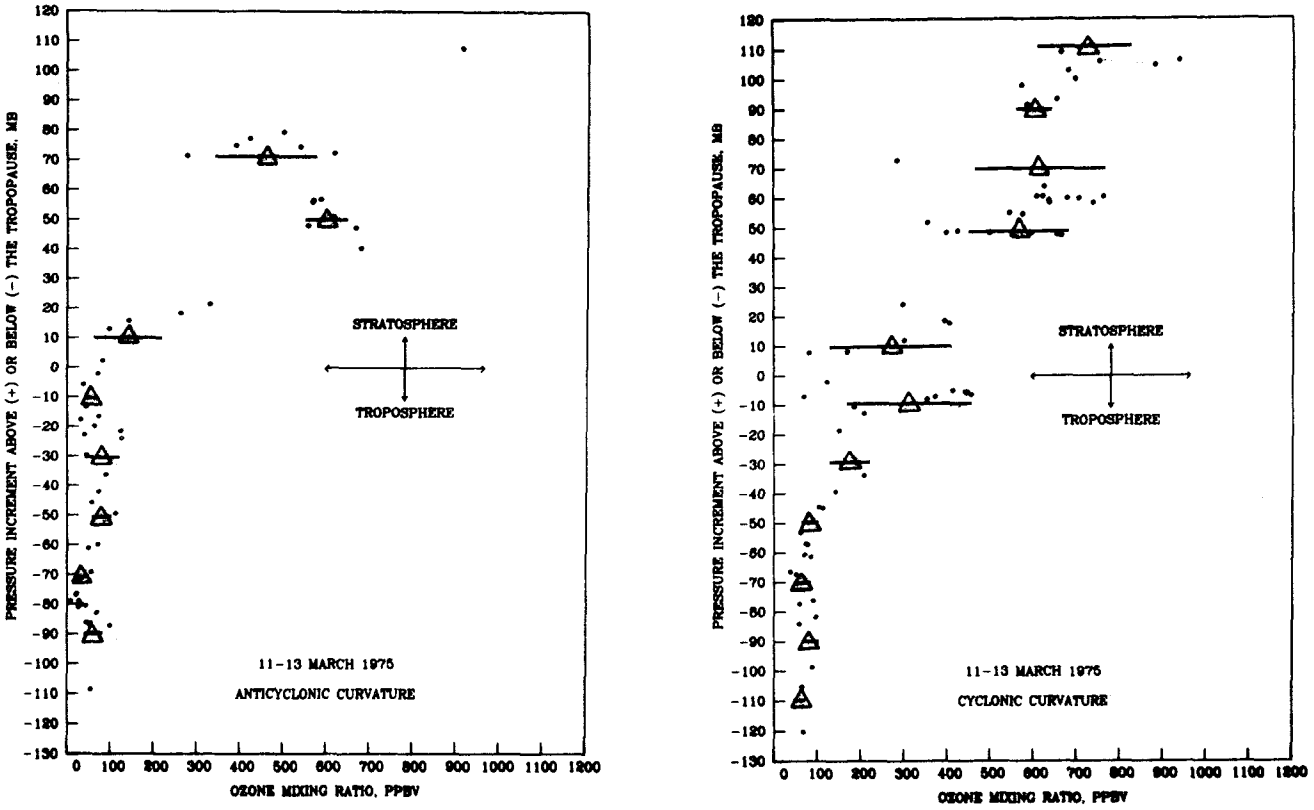

Figure 2. Vertical profile plots of ozone made aboard a GASP-equipped Pan Am 747 airliner, westbound with 8 intermediate stops from the U.S. West Coast to Europe. Data were recorded between 11-13 March 1975 and stratified for analysis according to curvature of the streamlines. 20-mb layer mean ozone amounts (triangles) and standard deviations (horizontal lines) have been entered as well.

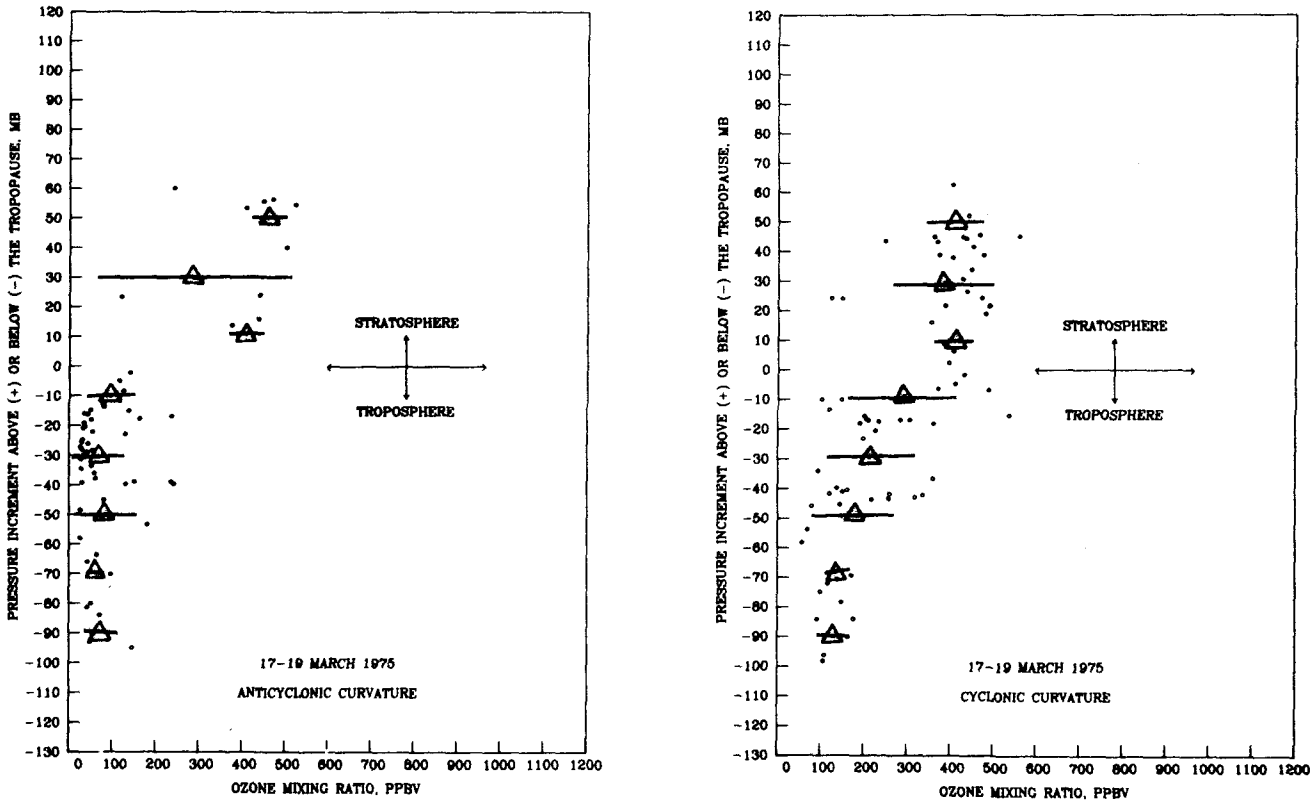

Figure 3. As in Figure 2, but for an eastbound Pan Am flight from New York to San Francisco via Europe, the Middle and Far East. Observations from 17-19 March 1975.

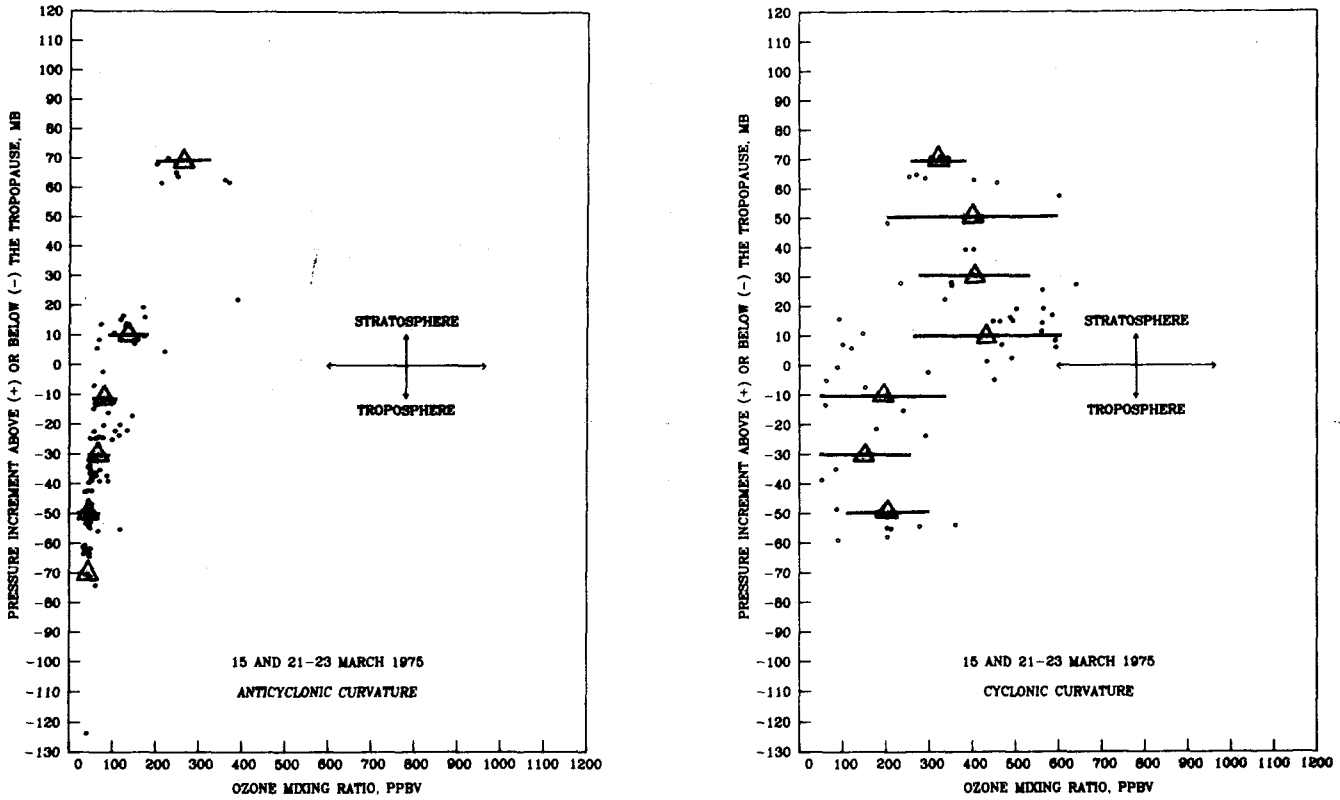

Figure 4. As in Figure 2, but for a sequence of four trans-Atlantic crossings between New York and London. Observations from 15 and 21-23 March 1975.

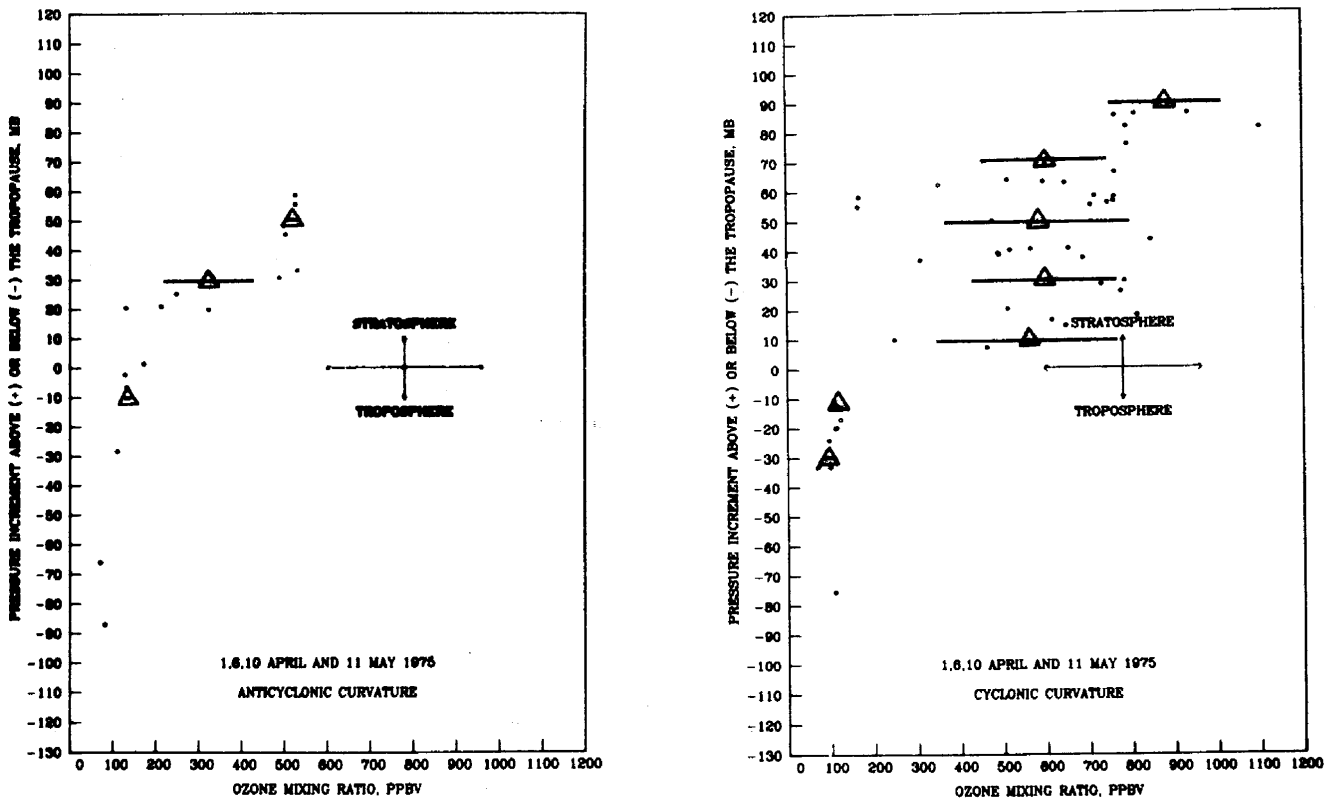

Figure 5. As in Figure 2, but for selected flights aboard the United Airlines 747 airliner over the contiguous United States. Observations from 1, 6, and 10 April and 11 May 1975.

APPENDIX

CALCULATION OF STREAMLINE CURVATURE FROM THE GASP DATA TAPES

by

Albion D. Taylor

In the analysis of data presented on the Global Atmospheric Sampling Program tapes, it is useful to stratify data according to some assumed indicator of the synoptic scale flow pattern in which the data was taken. One measure of the wind flow features can be obtained from the curvature of the streamlines, cyclonic curvature in the Northern Hemisphere generally correlating with unstable conditions and anticyclonic curvature with stable conditions. Accordingly it would be of value to have a means of calculating such curvature from the available data as recorded by the aircraft.

Unfortunately, it is not in general possible to obtain precise measurements of curvature from the available data, but one must be content with an estimate which becomes more or less reliable as the aircraft course and the streamline in question become parallel.

The data on the GASP tape relevant to the calculation of streamline curvature are the wind speed, direction, and the aircraft position as a function of time. The wind direction, of course, gives us by definition the direction tangent to the streamline. The streamline curvature is then the rate at which that direction changes with distance along the streamline. It is not sufficient, however, to take two successive measurements of wind direction, subtract and divide by the distance covered between readings, for several reasons.

In the first place, the reports of wind direction are in degrees measured from North, and the direction of North itself changes following the aircraft

path. This effect is most pronounced at high latitudes, and must be accounted for. More fundamentally, however, the two successive measurements will be made on separate streamlines, unless the aircraft happens to be flying directly upwind or downwind, and the definition of curvature requires two measurements on the same streamline.

In order to relate the measurements on the second streamline to those that would have been made on the original streamline, we would need more information on the structure of the wind field than can be obtained directly from the GASP data. More precisely, we need a linear combination of the divergence and the vorticity of the winds at the point of measurement, and since the coefficients of the linear combination involve the relative path of aircraft and streamline, in practice we need both divergence and vorticity. However, evaluations of neither divergence nor vorticity can be made from the data on a single flight track, but require in addition measurements made simultaneously at some distance away from the aircraft.

Recognizing that no evaluation of divergence or vorticity can be made from the aircraft data, in our program we arbitrarily set both equal to zero. In the present paper, we will retain the terms, however, so that an evaluation can be made of their importance in individual cases.

We first consider the simplest question, that of allowing for the variation in the direction of North.

Suppose two successive measurements are made at points A and B, at latitudes and longitudes ϕ, λ and $\phi+\Delta\phi$, $\lambda+\Delta\lambda$ (cf. Fig. A-1). The two points are a distance Δs apart. Now, consider the great circle path through

A and B, and the great circles (meridians) through A and B to the North Pole (N). The angles Ψ and $\Psi + \Delta\Psi$ made by AB with the local meridians NA and NB represent the local direction of AB with respect to North; the change $\Delta\Psi$ is the change in the direction of North along the great circle path AB. The figure ABN represents a spherical triangle; its sides in angular (radian) measurement are $\frac{\pi}{2} - \phi$, $\frac{\pi}{2} - \phi - \Delta\phi$, and $\Delta S/R$ where R denotes the radius of the Earth, and we may apply the sine and cosine laws of spherical trigonometry to find

$$\left.\begin{aligned} \sin(\phi + \Delta\phi) &= \sin\phi \cos(\Delta S/R) + \cos\phi \sin(\Delta S/R)\cos\Psi \\ \sin\Psi\cos\Psi &= \sin(\Psi + \Delta\Psi)\cos(\phi + \Delta\phi) \end{aligned}\right\} \quad (1)$$

After expanding, and dropping terms of second order in $\Delta\Psi$, $\Delta\phi$, and $\Delta S/R$, this becomes

$$\cos\phi\,(\Delta\phi - \Delta S/R(\cos\Psi)) = 0$$

$$\cos\Psi(\cos\phi)\Delta\Psi - \sin\phi\,(\sin\Psi)\Delta\phi = 0$$

or finally, eliminating $\Delta\phi$, and letting $\Delta\Psi$, ΔS tend to zero,

$$\frac{d\Psi}{ds} = \frac{\sin\Psi}{R} \cdot \tan\phi \qquad (2)$$

which expresses the rate by which the direction of North changes as a great circle path is traversed. It should be noted that this term can be quite significant at higher latitudes; at latitude 45^0, the term is important for streamlines with radius of curvature as tight as 300 km.

Because of the appearance of the tangent of latitude term, the differential form (2) for the rotation rate of the Northward direction is not a good starting place for finite difference formulations, at high latitudes. In programming the finite difference formulations for analysis of the GASP

data, we will proceed by a direct solution of equation (1) to find $\Delta\Psi$, as explained in greater detail later.

We now consider the question of how to find the streamline curvature using points on different streamlines. To separate the problems already considered, we will assume a coordinate system not necessarily related to the latitude-longitude system. Let the x-axis be the great circle route through two successive wind measurements. (If the aircraft is flying a great circle route, this means the aircraft is flying along the x-axis. Otherwise, the x-axis is a chord of the path of the aircraft, or tangent to the aircraft route in the limit of the differential forms.)

The y-axis taken to be the great circle through the first observation normal to the x-axis, and the other coordinate lines are great circles through one or the other axes. (This yields a geodesic coordinate system).

Using this coordinate system, let $W(x,y)$ denote the wind speed, $\eta(x,y)$ the direction <u>from</u> which the wind is coming, measured counterclockwise from the x-axis in radians, (cf. Fig.A-2), and let $U(x,y) = -W\cos(\eta)$, $V(x,y) = -W\sin(\eta)$ the components of wind in the x- and y- directions, respectively.

We assume that the wind fields do not change appreciably in the time period between observations, so that we may ignore the temporal part of the analysis, and we assume the distances travelled in this time are sufficiently small that we may ignore any differences between our coordinates and a Cartesian system.

We wish to find the curvatures of the streamlines, which are curves maintaining an angle η to the x-direction at every point, and the curvatures are therefore the rates of change of η with distance, taken in the direction

of the streamline, and are given by

$$\frac{d\eta}{ds} = \frac{\partial \eta}{\partial x}\frac{dx}{ds} + \frac{\partial \eta}{\partial y}\frac{dy}{ds} = -\cos\eta\,\frac{\partial \eta}{\partial x} - \sin\eta\,\frac{\partial \eta}{\partial y} \qquad (3)$$

where we take s for distance downwind along the streamline.

Now, because our data are measured along the x-axis, we know all the derivatives with respect to x directly, and none of the derivatives with respect to y. It follows that (3) will give us our desired streamline curvature exactly and directly, when and only when $\sin(\eta) = 0$, i.e., when the aircraft is flying directly upwind or downwind.

In other cases, we must find an estimate for the y- derivatives. It is here that we need information on the divergence and vorticity of the wind field. We write our required derivative in the form

$$\frac{\partial \eta}{\partial y} = \cos\eta\,\frac{\partial}{\partial y}(\sin\eta) - \sin\eta\,\frac{\partial}{\partial y}(\cos\eta)$$

$$= \frac{u}{w}\frac{\partial}{\partial y}\left(\frac{v}{w}\right) - \frac{v}{w}\frac{\partial}{\partial y}\left(\frac{u}{w}\right) = \frac{1}{w^2}\left(u\frac{\partial v}{\partial y} - v\frac{\partial u}{\partial y}\right)$$

On expressing the invariants δ, the divergence of the wind field, and ζ, the curl of the wind field, in the form

$$\delta = \frac{\partial u}{\partial x} + \frac{\partial v}{\partial y} \quad , \quad \zeta = \frac{\partial v}{\partial x} - \frac{\partial u}{\partial y}$$

and eliminating the y-derivatives, we have

$$\frac{\partial \eta}{\partial y} = \frac{1}{w}\left(\frac{u}{w}\cdot\delta + \frac{u}{w}\zeta - \frac{u}{w}\frac{\partial u}{\partial x} - \frac{v}{w}\frac{\partial v}{\partial x}\right)$$

After eliminating the components, this becomes

$$\frac{\partial \eta}{\partial y} = \frac{1}{w}\left(\delta\cos\eta + \zeta\sin\eta - \frac{\partial w}{\partial x}\right)$$

On substituting in (3), our final expression for curvature, in our local x-y coordinate system, is

$$K = \frac{d\eta}{ds} = -\cos\eta \cdot \frac{\partial \eta}{\partial x} + \frac{\sin\eta}{w}\left(\frac{\partial w}{\partial x} - \delta\cos\eta - \zeta\sin\eta\right) \qquad (4)$$

The final stage is to convert back from the local coordinate system to the global one of latitude and longitude. In so doing, we note that W, δ , and ζ are invariants and do not change in the transformation, while the derivatives with respect to x are simply derivatives with respect to distance along the aircraft track and will be so written. η is the angle between the down range aircraft track and the upwind streamline, and may be obtained from the recorded wind direction ν and the derived aircraft track direction ψ through (cf. Fig. A-3)

$$\eta = 2\pi + \psi - \nu$$

Using this relation, and equation (2), equation (4) becomes

$$K = \cos(\psi-\nu)\left(\frac{d\nu}{ds_a} - \frac{d\psi}{ds_a}\right) + \frac{\sin(\psi-\nu)}{W}\left(\frac{dw}{ds_a} - \delta\cos(\psi-\nu) - \zeta\sin(\psi-\nu)\right) \qquad (5)$$

$$= \cos(\psi-\nu)\left(\frac{d\nu}{ds_a} - \frac{\sin\psi}{R}\tan\phi\right) + \frac{\sin(\psi-\nu)}{w}\left(\frac{dw}{ds_a} - \delta\cos(\psi-\nu) - \zeta\sin(\psi-\nu\right.$$

where we have written d/ds_a to denote differentiation with respect to distance along the aircraft track.

Equation (5) represents the curvature expressed in global coordinates, in terms of the data available on the aircraft; plus divergence and curl, in a differential form. The data from the GASP program is given at finite intervals, of course, and a finite difference formulation is of importance

as well. At higher latitudes, the behavior of the $d\Psi/ds_a$ terms is such that a direct approximation to (5) is not appropriate, and the finite difference scheme we use will instead be derived in parallel to the above derivation.

The key to the finite difference formulation is a subroutine, ARCLBR, developed by the author at the Air Resources Laboratories. By providing the latitude and longitude of points A and B (cf. Fig. A-1) as input, the subroutine delivers the bearing Ψ, at A, of the great circle path AB from North, as well as the distance along the great circle path from A to B as output. By reversing the order of the arguments, we may obtain instead the bearing of the great circle from B to A, i.e., $\Psi + \Delta\Psi \pm 180^o$. A FORTRAN listing of ARCLBR appears as Table A-1.

From the GASP data tape, we obtain readings of latitude, longitude, wind speed, and wind direction, indexed by n, say: $\phi_n, \lambda_n, w_n, \nu_n$. On calling ARCLBR, first with $(\phi_{n-1}, \lambda_{n-1}, \phi_n, \lambda_n)$, then with $(\phi_n, \lambda_n, \phi_{n-1}, \lambda_{n-1})$, we obtain $\Delta s_n, \Psi_{n-1,n}$ and $\Psi_{n,n-1}$, the latter two being the bearings of point P_n: (ϕ_n, λ_n) as seen from P_{n-1}: $(\phi_{n-1}, \lambda_{n-1})$, and P_{n-1} as seen from P_n.

In view of the relation between η, Ψ and ν, we may then write the difference

$$\Delta\eta_{n,n-1} = \mathcal{R}(\nu_{n-1} - \nu_n - \Psi_{n-1,n} + \Psi_{n,n-1} + 180^o) \cdot \frac{\pi}{180}$$

where the function $\mathcal{R}$ denotes reduction, modulo 360, to a number between -180 and 190. When $\Delta\eta_{n,n-1}$ is divided by Δs_n, the result is a finite difference

expression for the term $\frac{\partial \eta}{\partial x}$ in (4).

The finite difference expression for the other derivative in (4) is chosen more conventionally as

$$\frac{\partial w}{\partial x} \sim \frac{w_n - w_{n-1}}{\Delta S_n}$$

There two expression actually correspond to the leg from P_{n-1} to P_n, and constitute "backward difference" approximations to the derivative at point P_n. Similar "forward difference" approximations may be defined using the data at P_n and P_{n+1} as

$$\frac{\partial \eta}{\partial x} \sim \frac{\Delta \eta_{n+1,n}}{\Delta S_{n+1}} = \mathcal{R}\left(\frac{\gamma_n - \gamma_{n+1} + \psi_{n+1,n} - \psi_{n,n+1} + 180)}{\Delta S_{n+1}}\right) \times \frac{\pi}{180}$$

and

$$\frac{\partial w}{\partial x} \sim \frac{w_{n+1} - w_n}{\Delta S_{n+1}} .$$

The two difference types are combined into a less biased "centered difference" approximation by forming a weighted-average using weights ΔS_n and ΔS_{n+1}:

$$\frac{\partial \eta}{\partial x} \sim \frac{1}{\Delta S_n + \Delta S_{n+1}}\left(\Delta S_{n+1} \frac{\mathcal{R}(\gamma_{n-1} - \gamma_n - \psi_{n-1,n} + \psi_{n,n-1} + 180)}{\Delta S_n} \cdot \frac{\pi}{180} + \Delta S_n \frac{\mathcal{R}(\gamma_n - \gamma_{n+1} - \psi_{n,n+1} + \psi_{n+1,n} + 180}{\Delta S_{n+1}} \cdot \frac{\pi}{180}\right)$$

$$\frac{\partial w}{\partial x} \sim \frac{1}{\Delta S_n + \Delta S_{n+1}}\left(\Delta S_{n+1}\left(\frac{w_n - w_{n-1}}{\Delta S_n}\right) + \Delta S_n\left(\frac{w_{n+1} - w_n}{\Delta S_{n+1}}\right)\right)$$

The remaining terms in (4) are approximated by the given values, w_n

and γ_n, for the wind speed and direction at point P_n, and by the aircraft track direction Ψ_n at point P_n. The latter is evaluated as a weighted-average of $\Psi_{n-1,n}$ and $\Psi_{n,n+1}$ in the following manner:

$$\Psi_n = \Psi_{n-1,n} + \frac{1}{\Delta S_n + \Delta S_{n+1}} \left(\mathcal{R} (\Psi_{n,n+1} - \Psi_{n-1,n}) \Delta S_n \right)$$

the reduction modulo 360 being required to ensure a rotation from one value to the other in the direction involving the lesser arc.

Unfortunately, the remaining two terms in (4), the divergence δ and the vorticity ζ, being descriptions of the two-dimensional structure of the wind field, cannot be obtained from the one-dimensional data available from the aircraft data. Our only practical choice is to assume them both zero in our reported "streamline curvature." Should such data become available from some other source, equation (4) demonstrates how to correct the reported values using them.

We have some general comments on interpretation of the formula for curvature and our reported values.

(1) Using the definition (equation (3)) of curvature and Fig. A-1. we note that $K = \frac{d\eta}{ds}$ is <u>greater</u> than zero when the streamline curves to the <u>left</u> in a <u>downwind</u> direction; it is <u>less</u> than zero when the streamline curves to the <u>right</u> in the downwind direction. In the Northern Hemisphere, these curvatures represent cyclonic and anti-cyclonic curvatures, respectively.

(2) Rather than report the curvature, in radians per kilometer, we report the <u>radius</u> of curvature, in kilometers. This is simply the inverse of the curvature itself, but is rather more directly comparable

with lengths on a map. This poses, however, a problem for places where a streamline is only very slightly curved, if at all (such as an inflection point). In such a case, the radius of curvature is reported as "zero" (though it is actually infinite) and another indicator is given, to be described below.

(3) If we consider the case where the aircraft is moving directly downwind ($\eta = 0^0$) or upwind ($\eta = 180^0$), and examine equation (4), we find the equation reduces to the first term, which is precisely the definition (equation (3)) of the curvature. In this case, then, we have directly a measurement of streamline curvature. The remaining terms of (4) must be regarded as corrections to be applied when the aircraft crosses streamlines at an angle, and are rather less reliable. The first of the correction terms, namely $\frac{1}{W} \frac{\partial W}{\partial x}$, may be understood as follows: consider a wind field whose streamlines are concentric circles and which is irrotational ($\zeta = 0$) and non-divergent ($\delta = 0$). Then $W = \Gamma/r$ where Γ is a constant and r the distance to their common center. If the aircraft flies directly to or from the center, i.e., normal to streamlines, then $\frac{1}{W} \frac{\partial W}{\partial x} = \pm \frac{1}{W} \frac{\partial W}{\partial r} = \pm \frac{1}{r}$, which is precisely the curvature of the streamline being crossed. In the real atmosphere, physical forces will intervene to produce vorticity or divergence before the infinite wind speeds can appear at the center ($r = 0$), and the remaining correction terms in (4) will be needed. Because the correction terms are considered somewhat less reliable in the curvature calculations, a measure of its relative contribution is made and printed as a percentage. This measure is simply the ratio of the magnitude of the first term to the sum of the magnitude of the two

terms. The nearer to 100%, the greater the contribution of the first term, and presumably the more reliable the estimate.

(4) In three cases, the meaning of the percentage figure is modified from that given above. In all cases, the reported "radius of curvature" is zero. The first case is when the radius is too large to print out; this case is indicated by changing the sign of the percentage figure to minus. In the second case, the radius of curvature is missing because the aircraft did not travel sufficiently far between readings for a reliable calculation of ΔS_n or of ΔS_{n+1}. This case, which occurs when the samples are taken in the limit mode, is indicated with "percentage" figure of -200%. The final case concerns the first and last data points of a flight, neither of which is the center of a triple of data points, and for which no "centered finite difference" form can be formulated. In this case, both the radius of curvature and "percent" figure are given as zero.

(5) In the real atmosphere, the values of vorticity and divergence encountered depend on the season, altitude, latitude, and the specific meteorological situation. The order of magnitude of relative vorticity generally agrees with the Coriolis parameter it is conveniently measured in units of 10^{-5} sec^{-1}. At a typical flight altitude of 12 gpkm, ζ might range from -12 to +12 x 10^{-5} sec^{-1} in winter; half that much in the summer. The extreme values tend to occur in the jet streams, where the higher velocities (up to 70 mps) tend to reduce the effect on curvature. A sample of a moderately large value for ζ would then be 10 x 10^{-5} sec^{-1}, and if we then assume a similar value for divergence and a wind

speed of 50 m s^{-1}, and a most unfavorable value for η, an error in curvature would appear corresponding to a radius of curvature of 500 km. This is, certainly comparable to the x curvature term from the term $\frac{d\Psi}{ds}$ of equation (2), for latitudes up to 70^{o}.

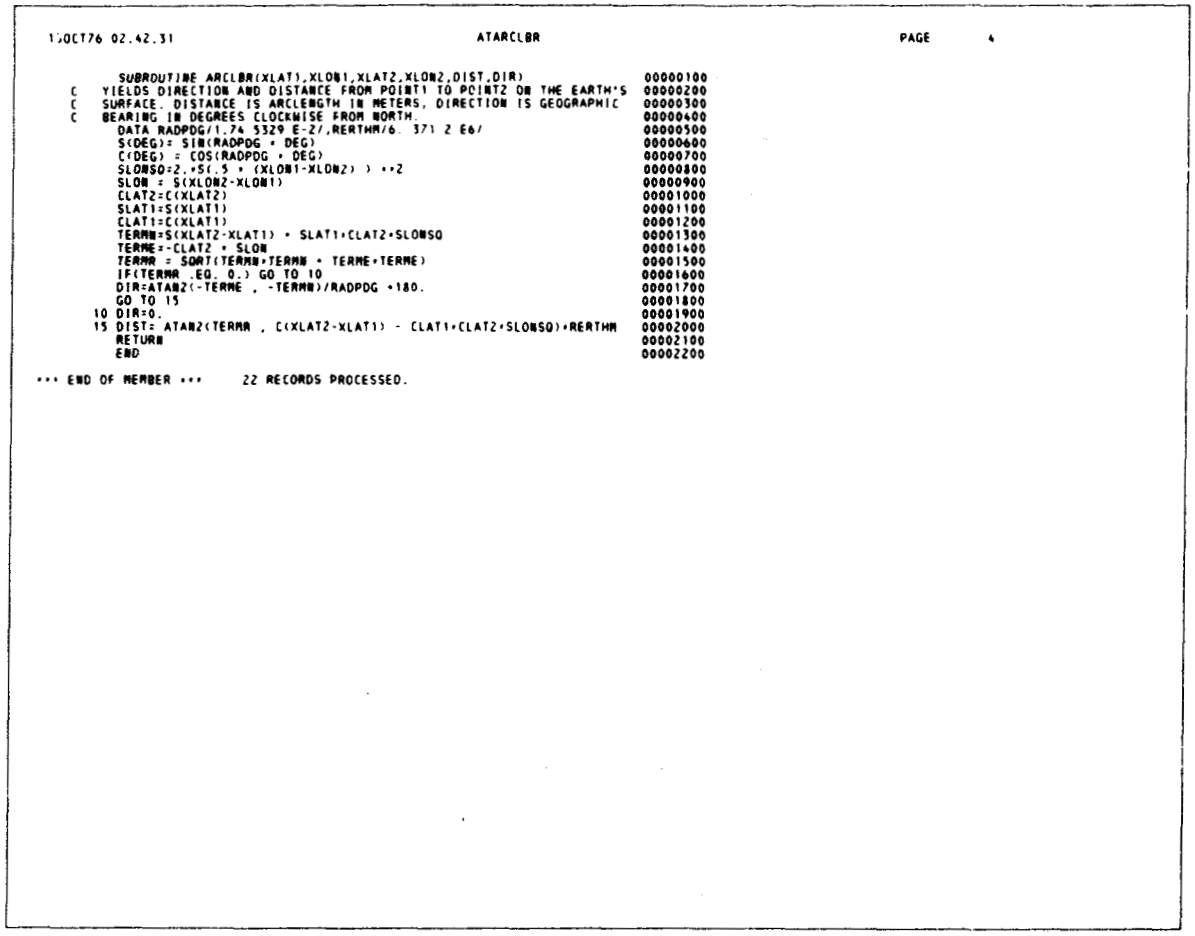

```
15OCT76 02.42.31                    ATARCLBR                              PAGE      4

      SUBROUTINE ARCLBR(XLAT1,XLON1,XLAT2,XLON2,DIST,DIR)                00000100
C   YIELDS DIRECTION AND DISTANCE FROM POINT1 TO POINT2 ON THE EARTH'S   00000200
C   SURFACE. DISTANCE IS ARCLENGTH IN METERS, DIRECTION IS GEOGRAPHIC    00000300
C   BEARING IN DEGREES CLOCKWISE FROM NORTH.                            00000400
      DATA RADPDG/1.74 5329 E-2/,RERTHM/6. 371 2 E6/                     00000500
      S(DEG)= SIN(RADPDG * DEG)                                          00000600
      C(DEG) = COS(RADPDG * DEG)                                         00000700
      SLONSQ=2.*S( .5 * (XLON1-XLON2) ) **2                              00000800
      SLON = S(XLON2-XLON1)                                              00000900
      CLAT2=C(XLAT2)                                                     00001000
      SLAT1=S(XLAT1)                                                     00001100
      CLAT1=C(XLAT1)                                                     00001200
      TERMN=S(XLAT2-XLAT1) * SLAT1*CLAT2*SLONSQ                          00001300
      TERME=-CLAT2 * SLON                                                00001400
      TERMR = SQRT(TERMN*TERMN + TERME*TERME)                            00001500
      IF(TERMR .EQ. 0.) GO TO 10                                         00001600
      DIR=ATAN2(-TERME , -TERMN)/RADPDG +180.                            00001700
      GO TO 15                                                           00001800
   10 DIR=0.                                                             00001900
   15 DIST= ATAN2(TERMR , C(XLAT2-XLAT1) - CLAT1*CLAT2*SLONSQ)*RERTHM    00002000
      RETURN                                                             00002100
      END                                                                00002200

*** END OF MEMBER ***     22 RECORDS PROCESSED.
```

Table A-1. FORTRAN listing of subroutine ACRLBR used at the Air Resources Laboratories. Two points on the earth's surface are program inputs and the direction and distance from the first point to second are program outputs.

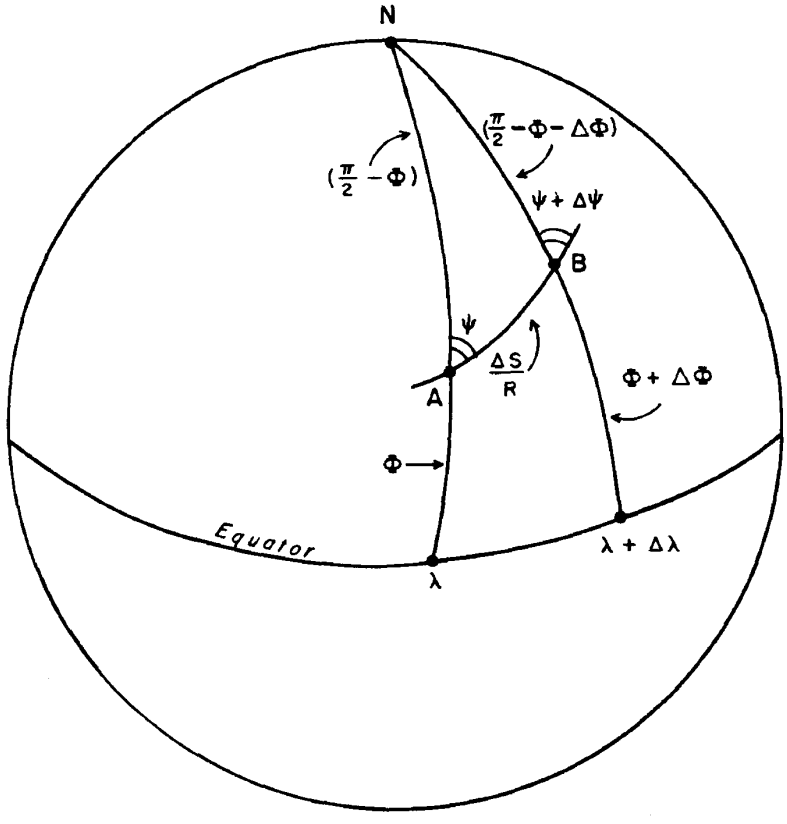

Fig. A-1. Spherical trigonometric representation of a great circle between two successive observation points, A and B. The latitudes and longitudes of these points are (ϕ,λ) and $(\phi+\Delta\phi)$, $(\lambda+\Delta\lambda)$. The change of direction of true north along AB is ψ, a change which must be evaluated in the general streamline curvature formula. See text for explanation.

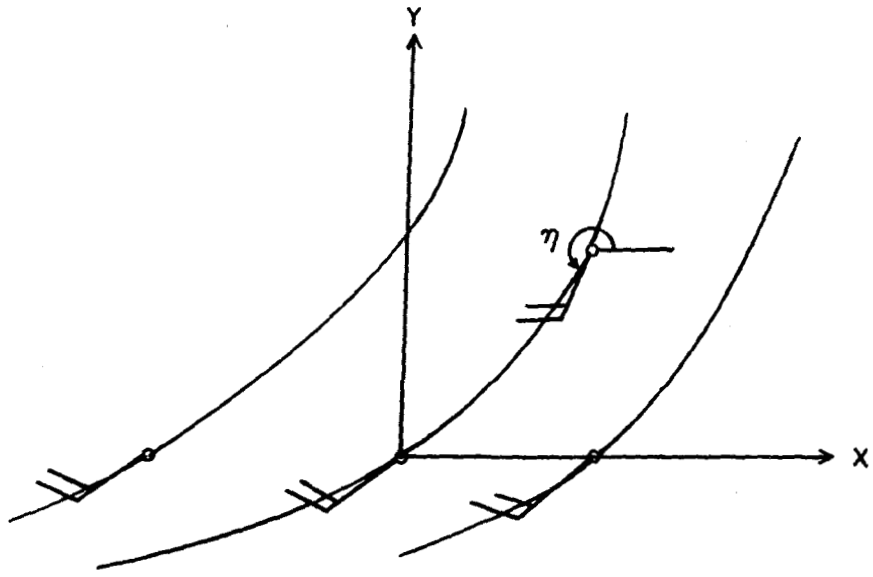

Fig. A-2. Local geodesic coordinate system in which the x-axis represents a great circle flight route between any two successive measurements. The y-axis is a great circle through the first observation and is normal to the abscissa. Angle η is the direction from which the wind is coming. See text for explanation.

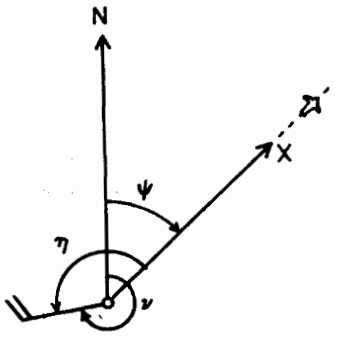

Fig. A-3. Relationship between the local geodesic coordinate system of Fig. A-2 and the global (latitude-longitude) coordinate system of Fig. A-1. Angles are defined in the text.